Malaysian Journal of Analytical Sciences (MJAS)
Published by Malaysian Analytical Sciences Society

SURFACTANT FUNCTIONALIZATION OF MAGNETIC NANOPARTICLES: A STUDY ON THE PARTICLE SIZE DISTRIBUTION AND ZETA POTENTIAL AS A NANOFLUID TO IMPROVE THERMAL CONDUCTIVITY

(Perfungsian Surfaktan Nanopartikel Magnet: Kajian Mengenai Taburan Saiz Zarah dan Potensi Zeta Sebagai Bendalir Nano untuk Meningkatkan Kekonduksian Terma)

Cheah Ching Wei[1], Noorashikin Md. Saleh[1*], Nik Nur Atiqah Nik Wee[1], Beh Shiuan Yih[1], Ahmad Fazlizan[2], Farhanini Yusoff[3]

[1,2]Department of Chemical and Process Engineering,
Faculty of Engineering and Built Environment, Universiti Kebangsaan Malaysia,
43600 UKM Bangi, Selangor, Malaysia
[2]Institute of Solar Energy,
Universiti Kebangsaan Malaysia, 43600 UKM Bangi, Selangor, Malaysia
[3]Faculty of Science and Marine Environment,
Universiti Malaysia Terengganu, 21030 Kuala Nerus, Terengganu, Malaysia

[*]Corresponding author: noorashikin@ukm.edu.my

Received: 18 May 2022; Accepted: 15 September 2022; Published: 27 December 2022

Abstract

Solar energy has gained increasing popularity in the last decade, resulting in the development of photovoltaic/thermal (PV/T) systems to improve photovoltaic cell efficiency. Working fluid is one of the most important components in a heat transfer system. In this study, Fe_3O_4@Sylgard 309 nanoparticles were synthesized for nanofluid preparation. The stability and particle size of the nanofluid were analyzed using the dynamic light scattering method. Water-based nanofluid at pH 7 had the highest zeta potential compared to the same water-based nanofluid at different pHs ranging from 5.2 to 9.4. The nanofluid synthesized using cetyltrimethylammonium ammonium bromide and sodium dodecyl sulfate as the surfactant achieved better stability than the nanofluid synthesized without the addition of the surfactant. Ethylene glycol (EG)-based nanofluid had the highest zeta potential value of -2.54 mV compared to the water-based and polyethylene glycol (PEG)-based nanofluids. Nanoparticles in the PEG-based nanofluid remained suspended for two days and were better than the water-based and EG-based nanofluids. The improvement of the thermal conductivity of the metal oxide nanofluid compared to the conventional base fluid in previous studies was reviewed. The results showed that the thermal conductivity of nanofluid was higher than the base fluid up to 49.4%, indicating the potential for nanofluid applications in PV/T systems if the stability of the nanofluid can be improved.

Keywords: Ferum(III) oxide, magnetic nanoparticle, nanofluid, thermal conductivity, thermophysical property

Abstrak

Popularitи tenaga suria semakin meningkat sejak sedekad yang lalu dan menghasilkan pembangunan sistem fotovolta/terma (PV/T) untuk meningkatkan kecekapan sel fotovolta. Bendalir kerja adalah salah satu komponen terpenting dalam sistem pemindahan haba. Dalam kajian ini, nanozarah Fe_3O_4@Sylgard 309 telah disintesis untuk menyediakan cecair nano. Kestabilan dan saiz zarah cecair nano dianalisis menggunakan kaedah penyerakan cahaya dinamik. Bendalir nano berasaskan air pada pH 7 mempunyai potensi zeta yang paling tinggi berbanding dengan cecair nano berasaskan air yang sama pada pH berbeza antara 5.2 hingga 9.4. Kestabilan cecair nano yang disintesis menggunakan setiltrimetilammonium bromida dan natrium dodesil sulfat sebagai surfaktan adalah lebih baik iaitu -2.54 mV daripada cecair nano yang disintesis tanpa penambahan surfaktan. Bendalir nano berasaskan etilena glikol (EG) mempunyai nilai potensi zeta yang paling tinggi berbanding dengan cecair nano berasaskan air dan polietilena glikol (PEG). Nanozarah dalam cecair nano berasaskan PEG kekal terampai selama dua hari dan lebih baik daripada cecair nano berasaskan air dan EG. Peningkatan kekonduksian terma bagi cecair nano oksida logam berbanding dengan cecair asas konvensional dalam kajian terdahulu telah dikaji semula. Keputusan menunjukkan bahawa kekonduksian terma cecair nano adalah lebih tinggi daripada cecair asas sehingga 49.4% dan mempunyai potensi aplikasi cecair nano dalam sistem PV/T sekiranya kestabilan cecair nano dapat dipertingkatkan.

Kata kunci: Ferum(III) oksida, nanozarah magnet, bendalir nano, termal kekonduksian, sifat termofizik

Introduction

As global warming worsens due to the emission of greenhouse gases, the demand for energy consumption is expected to increase, particularly in the industrial sector. According to the data obtained from the International Energy Agency, the growth of energy demand between 2017 and 2018 was 4% in 2018, which was equivalent to 900 TWh. The demand is expected to increase continuously as climate change increases the demand for air conditioning and consumption in the industrial sector [1-3].

Although solar energy can be converted into electrical energy using photovoltaic (PV) cells, long-term exposure will increase the temperature of the cells. Proton transfer rate is hindered in a commercial solar panel [4]. Meanwhile, 30% of the industrial process and heating, ventilation, and air conditioning (HVAC) systems require temperatures below 100 ℃, which can be achieved using commercial solar thermal collectors [3]. Working fluids (e.g., thermal oil, water, and glycols) have been implemented in HVAC systems but with poor efficiency.

Based on previous studies, PV electrical efficiency could be enhanced by integration with a heat collection system. The PV electrical efficiency of a photovoltaic/thermal (PV/T) system using silicon carbide (SiC) nanofluid under different solar irradiance levels (400–600 W) was enhanced significantly in the range of 13.3%-13.9% compared to the PV electrical efficiency of the reference PV module without a heat collection system in the range of 5.2%-10.52%. Another study on a PV/T system using SiC nanofluid reported an increase in the electrical efficiency up to 24.1% compared to the PV system alone [7]. A study on a PV/T system showed that the overall energy efficiency increased by 76.6% and achieved an overall energy efficiency of 16.9% using titanium dioxide (TiO_2) nanofluid compared to water [8]. These findings highlight the potential application of nanofluid in the PV/T system.

Magnetic nanoparticles possess magnetic properties that ease recycling and adsorption in the heat transfer process. Magnetic nanoparticles consist of iron oxides, iron alloys, and ferrite-based nanoparticles [9,10]. Nanofluid is the colloidal suspension of nanoparticles in the base fluid. Several types of nanofluid have been synthesized using carbon nanotube, metal oxide, and silica nanoparticles [11-25]. Surfactants such as cetyltrimethylammonium bromide (CTAB), sodium dodecyl sulfate (SDS), sodium dodecylbenzene sulfonate (SDBS), and acetic acid have been used to reduce agglomeration and improve the stability of nanofluids. The dispersion stability of the nanoparticles in the liquid will affect the commercialization of the nanofluid as the sedimented particles might cause scaling in the pump [26].

Ghadiri et al. synthesized Fe_3O_4 nanofluid with a nanoparticle concentration up to 3 wt. %. Acetic acid

was added to the nanofluid and ultrasonicated for 30 min to stabilize the nanofluid. The nanoparticle size was 45 nm and the nanofluid was stable for a month. The electrical and thermal efficiency of the PV/T system using 3 wt. % Fe_3O_4 nanofluid recorded an improvement of 4.8% and 35%, respectively, compared to the PV/T system using distilled water [27].

In the author's previous research, metal oxide nanofluid known as adsorbent MNP-Sylgard 309 was synthesized for the extraction of pollutants from environmental samples [11]. The excellent results allowed the metal oxide nanofluid to be applied in a new research field, which is the application for improving thermal conductivity. This is because the behavior of the synthesized metal oxide nanofluid has the tendency to increase the heat transfer rate in a heat exchanger without increasing its size. This is due to the higher thermal conductivity of the nanofluid. This improvement will lead to a lower temperature requirement in the thermal conductivity of a solar collector.

In this study, Fe_3O_4 nanoparticles were synthesized using the chemical co-precipitation method. Iron oxide nanoparticles were modified using 3-(triethoxysilyl)propylamine (APTES) and surfactant Sylgard 309. Fe_3O_4@Sylgard 309 nanoparticles were dispersed in the base fluid using ultrasonication to stabilize the nanofluid. Later, Fe_3O_4@Sylgard 309 nanoparticles were synthesized at different pHs using different base fluids. The nanoparticles and nanofluid synthesized were characterized using the dynamic light scattering (DLS) method. The stability of Fe_3O_4@Sylgard 309 nanoparticles in the water at different pHs was analyzed and compared. Furthermore, the stability of Fe_3O_4@Sylgard 309 nanoparticles in different base fluids (polyethylene glycol (PEG), ethylene glycol (EG), and water) at similar pH with the addition of different surfactants was compared. A review of previous studies regarding the thermal conductivity of metal oxide nanofluid in solar collectors was performed and summarized. Fe_3O_4@Sylgard 309 nanoparticles are feasible to be explored as the metal oxide nanofluid to be added to the solar collector for improving thermal conductivity.

Materials and Methods

Materials and reagents

Methanol (99.7%), ammonia hydroxide (25%), APTES, acetic acid, CTAB, polyethylene glycol (PEG 1500), EG, and SDS were purchased from Merck (Darmstadt, Germany). Iron(III) chloride hexahydrate ($FeCl_3 \cdot 6H_2O$) and iron chloride tetrahydrate ($FeCl_2 \cdot 4H_2O$) were supplied by R&M Chemicals (Essex, UK). Deionized water (18.2 MΩ cm^{-1}) used in the nanoparticles and nanofluid preparation was produced by a Sartorius Milli-Q system.

Synthesis of Fe_3O_4 nanoparticles

First, 3.1736 g of $FeCl_2 \cdot 4H_2O$ and 7.5709 g of $FeCl_3 \cdot 6H_2O$ were dissolved in 320 mL of deionized water and stirred under inert conditions for 1 h at 80 °C. Then, 40 mL of aqueous ammonia was added to the mixture and stirred for 1 h under inert conditions before being cooled to room temperature. The synthesized blackish liquid containing magnetic nanoparticles was decanted using a permanent magnet and washed using hot water five times to obtain Fe_3O_4 nanoparticles.

Surface modification of Fe_3O_4 nanoparticles using APTES and Sylgard 309

Next, the Fe_3O_4 nanoparticle surface was modified using APTES. A total amount of 4.2252 g of Fe_3O_4 was dissolved in 150 mL ethanol (50%) and sonicated for 30 min. Then, 17 mL of APTES was added to the mixture and stirred under inert conditions for 2 h at 40 °C before being cooled to room temperature. The modified nanoparticles were decanted and washed using ethanol and deionized water a few times prior to drying for 24 h at 70 °C under vacuum conditions. Finally, 0.2 g of the modified nanoparticles was dispersed in 8 mL of Sylgard 309 and stirred under inert conditions for 24 h at 60 °C before being cooled to room temperature. The final product was decanted and washed with deionized water and ethanol before being dried under vacuum conditions for 24 h at 70 °C. The synthesized nanoparticles were characterized using a Malvern Nano-ZS particle size analyzer to determine their hydrodynamic size and zeta potential. The synthesis of the Fe_3O_4@Sylgard 309 nanoparticle is shown in Figure 1.

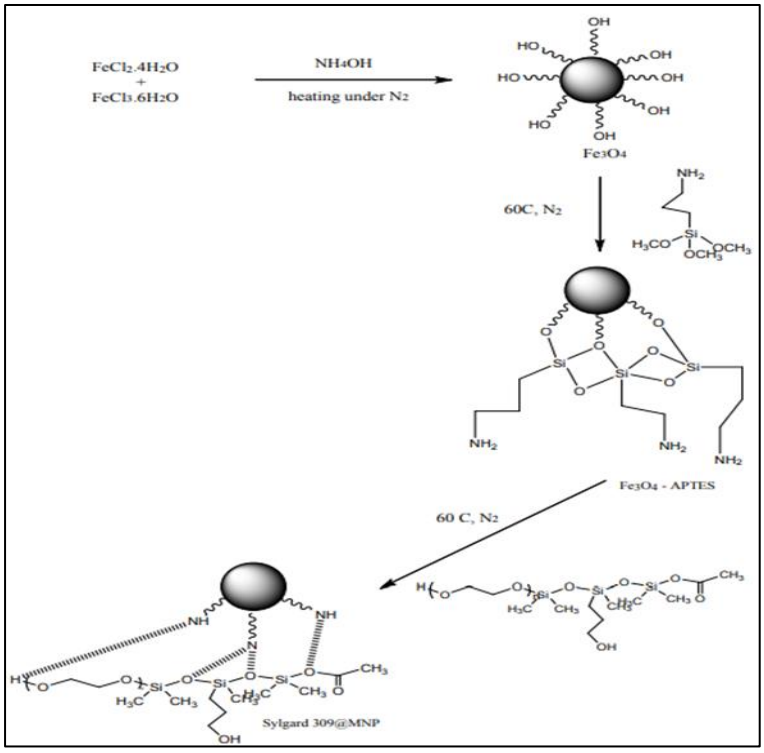

Figure 1. Synthesis of Fe_3O_4@Sylgard 309 nanoparticle [16]

Preparation of nanofluid

Nanofluid preparation was done by sonication (60 min) after adding the modified nanoparticles to the water with a concentration of 0.1 wt.%. Different types of nanofluids were synthesized using different base fluids (PEG, EG) and at different pHs (5.2, 5.9, 7.0, 8.4, 9.4). The dispersion stability and zeta potential of the nanofluids were determined using the Malvern Nano-ZS particle size analyzer.

Results and Discussion

Particle size distribution of synthesized nanoparticles

The results for the synthesis of Fe_3O_4 nanoparticles and surface modification of Fe_3O_4 nanoparticles using APTES and surfactant Sylgard 309 have been published [16]. The paper contains the results of the characterization of Fe_3O_4 nanoparticles coated with APTES and Sylgard 309. The current paper focuses on the application of Fe_3O_4 nanoparticles coated with APTES and Sylgard 309 by studying the particle size di stribution and zeta potential of the nanofluid to improve thermal conductivity. The particle size distribution result showed that the color of Fe_3O_4 changed from black to brown after modification using APTES. Then, the brown color of APTES-modified Fe_3O_4 nanoparticles using Sylgard-309 changed to dark brown. The surface-modified nanoparticle samples are shown in Figure 2. Changes in the color of Fe_3O_4 nanoparticles after surface modification were observed in previous studies [32, 33]. Fe_3O_4 surface modification was done without changing the nanoparticle core (i.e., Fe_3O_4). A study determined that the crystallinity was preserved even after surface modification based on the same peak intensity in the X-ray diffraction (XRD) diffractogram [16].

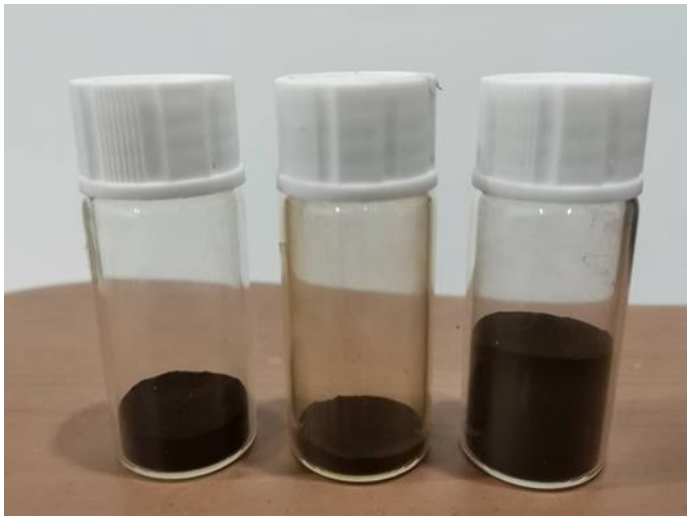

Figure 2. Fe_3O_4 nanoparticles synthesized (left) and modified using APTES (middle) and Sylgard 309 (right)

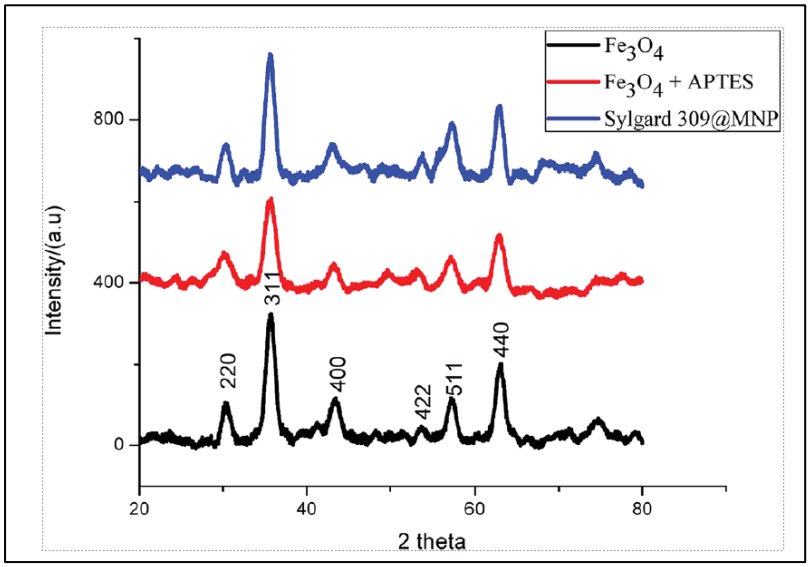

Figure 3. XRD patterns of Fe_3O_4 nanoparticles, Fe_3O_4 + APTES nanoparticles, and Sylgard 309@MNP [16]

In our previous study, XRD was used to identify the crystallinity of Fe_3O_4, Fe_3O_4 + APTES, and Sylgard 309@MNP. As shown in Figure 3, Fe_3O_4 exhibited good crystallinity with diffraction peaks appearing at the 2θ values of 30.42°, 35.59°, 43.59°, 53.63°, 57.50°, and 63.04°, which can be assigned to the (220), (311), (400), (422), (511), and (440) reflections of Fe_3O_4, respectively, which are similar to those of other previous studies [23, 24]. Furthermore, the spectra of Fe_3O_4 + APTES and Sylgard 309@MNP showed approximately identical characteristics of diffraction peaks, revealing that the surface modification of Fe_3O_4 did not change its crystalline phase. The lower intensity of the diffraction peaks was observed in the cases of Fe_3O_4 + APTES and Sylgard 309@MNP, which may be due to the presence of an amorphous layer of APTES and Sylgard 309 on Fe_3O_4 [16].

Based on the particle size distribution shown in Figure 4, the particle size of the synthesized Fe_3O_4 had two peaks, which were 862.2 nm with 89.1% of intensity and 90.53 nm with 10.9% of intensity. This revealed that the diameter of the synthesized nanoparticles was lower than 100 nm. However, there was another peak at 862.2 nm, which was due to agglomeration, and this increased the hydrodynamic size of the nanoparticles in the nanofluid.

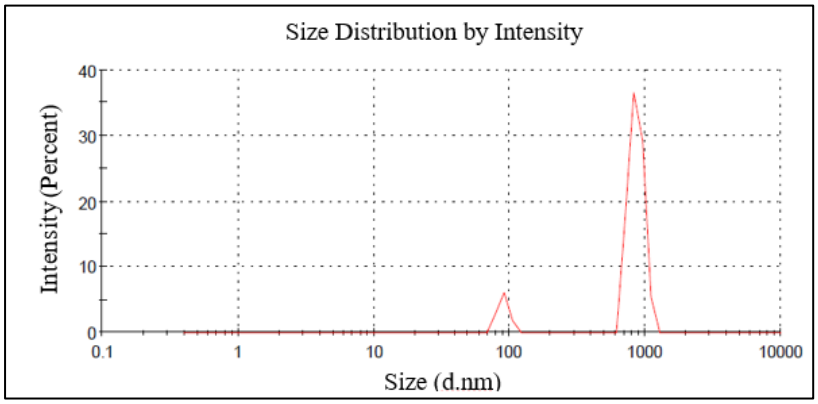

Figure 4. Particle size distribution of synthesized Fe_3O_4 nanoparticles

In the DLS method, an incident laser is generated, which is scattered by the nanoparticles in the colloidal suspension, causing constructive and destructive interference and also resulting in the fluctuation of the scattered light intensity. The fluctuation of the light intensity is then correlated to derive the hydrodynamic radius of the solid particle. The particle diameter detected using the DLS method is the hydrodynamic diameter of the solid particle, which is bounded by the slipping plane.

The slipping plane of the nanoparticle is affected by the aggregation and diffusion of the particle through the boundary of the hydrodynamic structure (slipping plane) into the internal layer [34]. Therefore, if the nanoparticle is not monodispersed in the nanofluid, then the particle size of each nanoparticle cannot be characterized accurately using the DLS method. This is due to the aggregation of nanoparticles in the colloidal suspension, which will result in inaccurate particle size measurement. The reported data of DLS and zeta potential were inaccurate in previous research of nanomedicine research [35].

In Figure 5, the result from DLS showed that the nanoparticles modified using APTES had a larger particle diameter of 1,817 nm. However, after the APTES-modified nanoparticles were characterized using Sylgard 309 (a non-ionic surfactant), the result in Figure 6 showed that the two peaks in the particle size were 73.32 nm with 7.8% of intensity and 482.4 nm with 92.2% of intensity. This proved that the particles modified using APTES caused the aggregation. The change in the particle size distribution could be affected by zeta potential and changes in the zeta potential might be caused by the shift of the slipping plane by molecules characterized on the core nanoparticle surface and also the displacement of the counter ion in the stern layer due to polymer adsorption on the core nanoparticles [36].

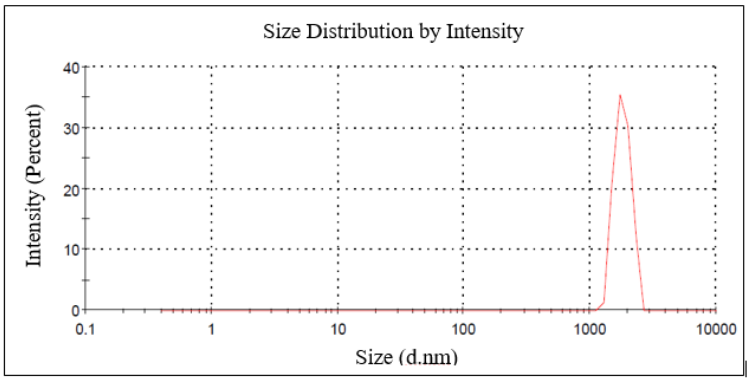

Figure 5. Particle size distribution of Fe_3O_4 nanoparticles modified using APTES

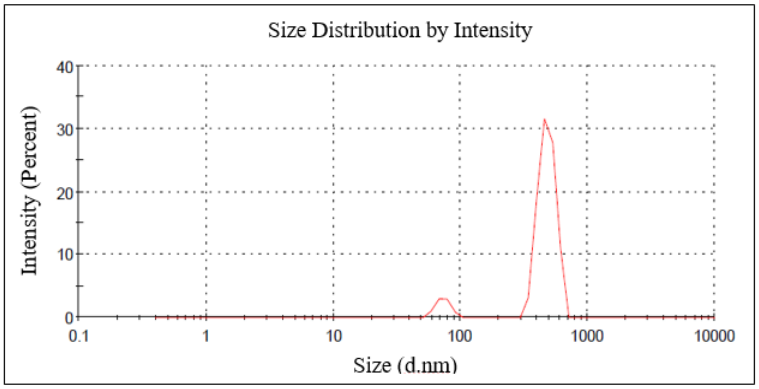

Figure 6. Particle size distribution of synthesized Fe_3O_4@Sylgard 309 nanoparticles

Zeta potential and stability of the synthesized nanofluid

Zeta potential is the parameter used to characterize the electric double layer on the solid/liquid interface. When an ionized solid particle is suspended in the liquid, it will be surrounded by liquid ions with the opposite charge to the surface of the solid particle. Both the solid particle and the liquid layer shell will move together through the liquid. The potential difference between the external liquid shell and the liquid is called zeta potential. Zeta potential is used to describe the behavior of the dispersion of particles in the colloidal system and the stability of the nanofluid [26, 37]. Abadeh et al. examined the effect of the type of surfactant, the amount of surfactant, and pH on nanofluid stability and magnetization [38].

This solid/liquid interface is the boundary of the hydrodynamic structure of the nanoparticles in the colloidal suspension and zeta potential is the potential difference between the internal layer and the external layer of the slipping plane, as shown in Figure 5 Zeta potential is an established parameter in determining the stability of nanoparticle dispersion in nanofluid against aggregation. Zeta potential higher than 30 mV or lower than -30 mV is considered a stable suspension due to charge stabilization between the nanoparticles with high electrostatic repulsive strength. Colloidal suspension with zeta potential higher than 40 mV or lower than -40 mV is considered as having good stability [34, 37].

Based on the zeta potential values measured using the DLS method in Table 1, it can be determined that none of the synthesized nanofluids had enough stability to be

considered as stable colloidal suspension. In the particle size distribution measurement, the results generated are similar to the particle size distribution in which the particle size is affected by the aggregation of the nanoparticles. This is because the particle size distribution increased as the aggregation increased. Furthermore, the pH value will affect the zeta potential of the nanofluid. The zeta potential will affect the dispersive ability of the nanoparticles in the nanofluid, resulting in nanoparticle aggregation. This is in good agreement with previous studies. Zeta potential is usually related to the time needed for the nanoparticles to sediment at the bottom of the nanofluid. The time needed for the nanoparticles to sediment in the nanofluid with a zeta potential value higher than 30 mV or lower than -30 mV is longer than the nanofluid with a zeta potential value closer to 0 mV.

Table 1. Zeta potential and nanoparticle size distribution of water-based nanofluids synthesized at different pHs

pH	**5.2**	**5.9**	**Intensity percentage (%)**	**7.0**	**Intensity percentage (%)**	**8.4**	**9.4**
Particle size, diameter (nm)	163.9	463.9	89.2	482.4	92.2	893.1	1,868
	-	111	10.8	73.32	7.8	-	-
Zeta potential (mV)	-5.56	-4.5	100	-12.4	100	-2.54	-2.62

The zeta potential value was the lowest at pH 7. As the pH value transitioned to a higher or lower value, the zeta potential increased and became closer to 0 mV. However, based on the observation, the sedimentation of the particles at pH 7 occurred earlier than other nanoparticles. This might be due to the nanoparticles being synthesized using Sylgard 309, which is a non-ionic surfactant. This result is in contrast with the statement that the closer the zeta potential value to 0 mV, the shorter the time needed for nanoparticle sedimentation to occur. However, it is still acceptable as the zeta potential of the synthesized nanofluid is not lower than -30 mV and is still considered an unstable nanofluid. The nanoparticles in all water-based nanofluids synthesized at different pHs were found to sediment at the bottom of the nanofluids in a day. Therefore, pH 9.4 was chosen as an optimum pH used for the subsequent study.

In Figure 7, the zeta potential of the water-based nanofluid without the addition of surfactant showed an apparent zeta potential of -5.8 mV, while the zeta potential of the water-based nanofluids synthesized with CTAB and SDS achieved the zeta potential values of 32.3 mV and -41.9 mV, as shown in Figures 8 and 9, respectively. Nanofluid stability improvement was achieved using CTAB and SDS as the surfactant. The zeta potential result of the synthesized nanofluid with CTAB was positive, while the zeta potential result with the addition of SDS was always negative. Both surfactants were able to stabilize the nanofluid as the zeta potential of the synthesized nanofluid was higher than 30 mV or lower than -30 mV. The zeta potential results are in good agreement with the data from previous studies. The time needed for nanoparticle sedimentation to occur in the nanofluids with the addition of CTAB and SDS was longer than the synthesized nanofluid without the addition of surfactant. However, the nanoparticles in the synthesized nanofluid were found to sediment at the bottom of the nanofluid in a day.

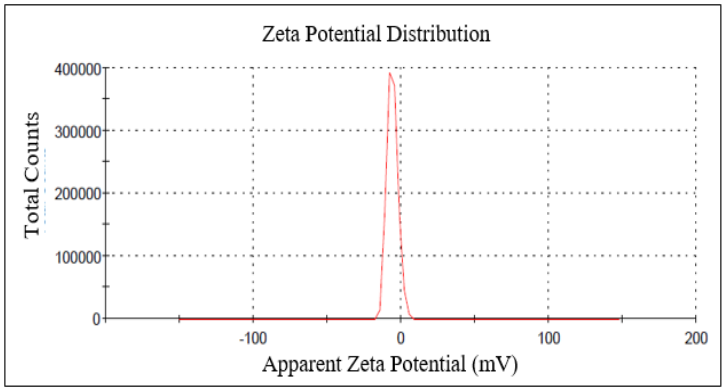

Figure 7. Zeta potential of water-based nanofluid synthesized without the addition of surfactant

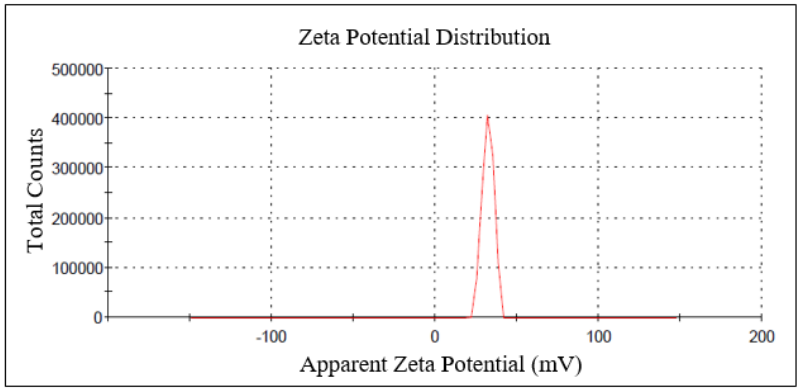

Figure 8. Zeta potential of water-based nanofluid synthesized with the addition of CTAB

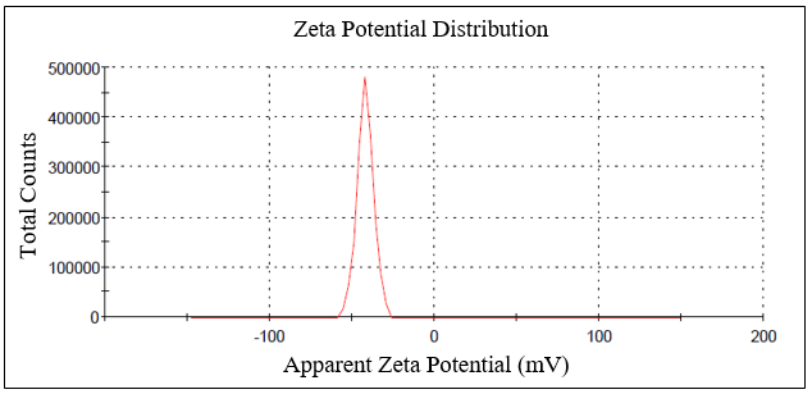

Figure 9. Zeta potential of water-based nanofluid synthesized with the addition of SDS

Nanofluids were synthesized using different base fluids of water, PEG, and EG without any addition of surfactant. Based on the data obtained in Table 2, it was found that the zeta potential value of water-based nanofluid was -2.62 mV, -14.7 mV for EG-based nanofluid, and 3.93 mV for PEG-based nanofluid. The water-based nanofluid recorded a zeta potential closest to zero, which means that it is highly unstable.

EG-based nanofluid was also highly unstable due to the similar zeta potential value to water-based nanofluid. EG-based nanofluid had a zeta potential value that was furthest away from 0 mV. However, based on the observation, nanoparticles in PEG-based nanofluid were able to remain suspended within two days, while the nanoparticles in water- and EG-based nanofluids were only able to remain suspended within one day. This is because PEG is a high viscosity base fluid. Sedimentation is caused by the resultant force acting on the nanoparticles from the stronger gravitational force than the drag force exerted on the nanoparticles by the base fluid [42].

The drag force in a high viscosity base fluid is stronger than a low viscosity base fluid. Therefore, the sedimentation time of the nanoparticles in PEG-based nanofluid was longer.

Table 2. Zeta potential values of nanofluids synthesized using different base fluids

Type of Base Fluid	Water-based at pH 9	EG-based	PEG-based
Zeta potential (mV)	-2.62	-14.7	3.93

Review of previous studies on nanofluid thermal conductivity in solar collectors

Based on previous studies, the application of metal oxide nanofluid in PV/T systems improved the energy generation efficiency compared to the PV/T system utilizing conventional base fluid or PV system alone. Several types of nanofluids from previous studies are summarized in Table 3.

Abareshi et al. synthesized Fe_3O_4 nanofluid using tetramethylammonium hydroxide as the surfactant. The study stated that nanofluid suspension with a zeta potential lower than -30 mV or higher than 30 mV was a stable nanofluid. The nanofluid had a zeta potential value of -41.7 mV, hence it was a stable nanofluid, and the thermal conductivity improvement was 11.5% when the volume fraction of the magnetic nanoparticles was 3 vol% at 40 °C [46].

Al-Shamani et al. prepared TiO_2 nanofluid to be implemented in a thermal collector system of an integrated PV/T module. Based on the results, the TiO_2 nanofluid had an improved thermal conductivity of 12.5% compared to water. The electrical efficiency of the PV/T system utilizing TiO_2 increased by 1% compared to the module utilizing water due to the lower module temperature after exposure to solar irradiation [6].

Based on the previous studies on thermal conductivity, it was shown that the PV/T system utilizing metal oxide nanofluid was able to gain up to 49.4% thermal conductivity improvement compared to the conventional base fluid. However, the results of thermal conductivity improvement of the nanofluid varied. This could be due to different methods used for measuring the thermal conductivity improvement of the nanofluid under different parameters, such as humidity and the surrounding temperature of the environment.

In previous research on magnetic actuated transfer systems, it was shown that it was possible to achieve overall exergy, heat transfer coefficient, and thermal efficiency improvement when the Fe_3O_4 nanofluid was under an alternating magnetic field. However, the difference in the data varied widely. Therefore, it is important to study this particular system to gain more data to determine if any additional factors may cause the discrepancies between these studies on magnetic nanofluids, as well as other nanofluids in heat transfer applications.

Table 3. Summary of thermal conductivity improvement of nanofluids in previous studies

Nanofluid	Concentration	Stabilization Process	Stabilization Analysis	Thermal Conductivity Improvement	Study
• Fe_3O_4/water	•1 wt.% •3 wt.%	• Surfactant – acetic acid • Ultrasonication – 30 min	• Stable in a month • Particle diameter = 45 nm	• No data	22
• TiO_2/water	•0.1 wt.%	• Surfactant – SDS • Ultrasonication bath – 3 h	• Stable in 3 days	• 1%	37
• TiO_2/water	•0.1 vol% •0.3 vol%	• Surfactant – PEG • Pressurized homogenization	• Stable for a month • Ratio of nanoparticle: surfactant = 1:2	• 6%	16
• Al_2O_3/water • CuO/water	•0.8 wt. %	• Surfactant –SDBS • pH: alumina = 8.0, Cu = 9.5	• Zeta potential higher than 40 mV	• Alumina: 15% • Cu: 18%	39
• Al_2O_3/water • CuO/water	•2–10 vol% •2–10 vol%	• Ultrasonication – 3 h	• Stable for a few days	• Alumina: 30% • Cu: 52%	40
• Fe_3O_4/water	•No data	• No data	• No data	• No data	41
• Fe_3O_4/ water	•0–3 vol%	• Surfactant – tetramethylammonium hydroxide	• No data	• 11.5% at 40 ℃	42
• TiO_2/water	•0–2 wt. %	• Ultrasonication	• No data	• 12.5%	6
• Fe_3O_4/water	•0%–0.1%	• No data	• Zeta potential = -46.3 mV	• 33.8% at 40 ℃	14

Conclusion

Fe_3O_4@Sylgard 309 nanoparticles were synthesized and used as the nanofluid to improve the stability and thermophysical properties of a solar collector. The stability and particle size of the nanofluid were analyzed using the DLS method. Water-based nanofluid at pH 7 had the highest zeta potential compared to the same water-based nanofluid at different pHs ranging from 5.2 to 9.4. The stability of the synthesized nanofluid using CTAB and SDS as the surfactant was better than the nanofluid synthesized without the addition of surfactant. EG-based nanofluid had the highest zeta potential value compared to the water- and PEG-based nanofluids. Nanoparticles in PEG-based nanofluid could remain suspended within two days, which were longer than water- and EG-based nanofluids. Therefore, PEG-based

nanofluid has the potential to be used in a solar collector because it has longer time to be effective as a fluid, which is related to the high conductivity in a solar system. The thermal conductivity improvement of the metal oxide nanofluid compared to conventional base fluid in previous studies was reviewed. The review showed that the thermal conductivity of nanofluid was higher than the base fluid up to 49.4%. This result highlights the potential of nanofluid applications in PV/T systems if the stability of the nanofluid can be improved.

Acknowledgement

We would like to express our gratitude to the Ministry of Higher Education Malaysia for the Fundamental Research Grant Scheme FRGS/1/2022/STG04/UKM/02/7.

References

1. IEA (2019). Global Energy & CO2 Status Report. 2019
2. Ritchie, H., and Roser, M. (2017). CO_2 and greenhouse gas emissions. *Renewable Energy.* 2017: pp. 1-10.
3. Dahlan, N. Y., and Ismail, M. F. A (2015). Review on solar thermal technologies for low and medium temperature industrial process heat. *Journal of Industrial Technology*, 23(1): 25-44.
4. Ibrahim, A., and El-Amin, A. (2012). Temperature effect on the performance of n-type c-Si film grown by linear facing target sputtering for thin film silicon photovoltaic devices. *Optoelectronics and Advanced Materials-Rapid Communications,* 6:73-77.
5. Jama, M., Singh, T., Gamaleldin, S. M., Koc, M., Samara, A., Isaifan, R. J. (2016). Critical review on nanofluids. *Journal of Nanomaterials,* 26: 6717624.
6. Al-Shamani, A. N., Sopian, K., Mat, S., Hasan, H. A., Abed, A. M., and Ruslan, M. (2016). Experimental studies of rectangular tube absorber photovoltaic thermal collector with various types of nanofluids under the tropical climate conditions. *Energy Conversion and Management,* 124: 528-542.
7. Al-Waeli, A. H., Sopian, K., Chaichan, M. T., Kazem, H. A., Hasan, H. A., and Al-Shamani, A. N. (2017). An experimental investigation of SiC nanofluid as a base-fluid for a photovoltaic thermal PV/T system. *Energy Conversion and Management,* 142, 547-558.
8. Said, Z., Sabiha, M., Saidur, R., Hepbasli, A., Rahim, N. A., Mekhilef, S., et al. (2015). Performance enhancement of a flat plate solar collector using titanium dioxide nanofluid and polyethylene glycol dispersant. *Journal of Cleaner Production,* 92: 343-353.
9. Yusoff, M. M., Yahaya, N., Saleh, N. M., and Raoov, M. (2018). A study on the removal of propyl, butyl, and benzyl parabens via newly synthesised ionic liquid loaded magnetically confined polymeric mesoporous adsorbent. *RSC Advances,* 8(45): 25617-25635.
10. Guo, T., Lin, M., Huang, J., Zhou, C., Tian, W., Yu, H., et al. (2018). The recent advances of magnetic nanoparticles in medicine. *Journal of Nanomaterials*, 2018: 7805147.
11. Noorashikin, M.S., Mohamad, S. and Abas, M. R. (2014). Extraction of parabens from water samples using cloud point extraction of non-ionic surfactant with beta-cyclodextrin as modifier. *Journal of Surfactants and Detergents*, 17: 747-758.
12. Yusoff, F., Khing, N. T., Hao, C. C., Sang, L. P., Muhamad, N. A. B., and Saleh, N. M. (2018). The electrochemical behavior of zinc oxide/reduced graphene oxide composite electrode in dopamine. *Malaysian Journal of Analytical Sciences,* 22(2): 227-237.
13. Noorashikin, M. S., Sohaimi, N. M., Suda, N., Aziz, H. Z., Zaini, S. R. M., Kandasamy, S., et al. (2017). The application of cloud point extraction in environmental analysis. *Journal Sustainability Science Management,* 12: 79-95.
14. Noorashikin, M., Mohamad, S., and Abas, M. (2016). Determination of parabens in water samples by cloud point extraction and aqueous two-phase extraction using high-performance liquid chromatography. *Desalination and Water Treatment,* 57(47): 22353-22361.

15. Norseyrihan, M. S., Noorashikin, M. S., Adibah, M., and Farhanini, Y. (2016). Cloud point extraction of methylphenol in water samples with low viscosity of non-ionic surfactant Sylgard 309 coupled with high-performance liquid chromatography. *Separation Science and Technology*, 51(14): 2386-2393.
16. Ariffin, M. M., Sohaimi, N. M., Yih, B. S., and Saleh, N. M. (2019). Magnetite nanoparticles coated with surfactant Sylgard 309 and its application as an adsorbent for paraben extraction from pharmaceutical and water samples. *Analytical Methods,* 11(32): 4126-4136.
17. Baker, I. (2018). Magnetic nanoparticle synthesis. *Nanobiomaterials*, 2018: 197-229.
18. Gonzalez-Carreno, T., Morales, M., Gracia, M., and Serna, C. (1993). Preparation of uniform γ-Fe_2O_3 particles with nanometer size by spray pyrolysis. *Materials Letters,* 18(3): 151-155.
19. Haiza, H., Yaacob, I., and Azhar, A. Z. A. (2018). Thermal conductivity of water-based magnetite ferrofluids at different temperature for heat transfer applications. *Solid State Phenomena,* 280: 36-42.
20. Moon, J.-W., Rawn, C. J., Rondinone, A. J., Love, L. J., Roh, Y., Everett, S. M., et al. (2010). Large-scale production of magnetic nanoparticles using bacterial fermentation. *Journal of Industrial Microbiology & Biotechnology*, 37(10): 1023-1031.
21. Safee, N. H. A., Abdullah, M. P., and Othman, M. R. (2010). Carboxymethyl chitosan− Fe_3O_4 nanoparticles: synthesis and characterization. *Malaysian Journal Analytical Sciences,* 14: 63-68.
22. Sugimoto, T., Wang, Y., Itoh, H., and Muramatsu, A. (1998). Systematic control of size, shape and internal structure of monodisperse α-Fe_2O_3 particles. *Colloids and Surfaces A: Physicochemical and Engineering Aspects,* 134(3): 265-279.
23. Sun, S., and Zeng, H. Size-controlled synthesis of magnetite nanoparticles. *Journal of the American Chemical Society*, 124(28): 8204-8205.
24. Wang, X., Zhuang, J., Peng, Q., and Li, Y. (2005). A general strategy for nanocrystal synthesis. *Nature*, 437(7055): 121-124.
25. Zhang, G., Liao, Y., and Baker, I. (2010). Surface engineering of core/shell iron/iron oxide nanoparticles from microemulsions for hyperthermia. *Materials Science and Engineering*, 30(1): 92-97.
26. Biehl, P., Von der Lühe, M., Dutz, S., and Schacher, F. H. (2018). Synthesis, characterization, and applications of magnetic nanoparticles featuring polyzwitterionic coatings. *Polymers*, 10(1): 91.
27. Ghadiri, M., Sardarabadi, M., Pasandideh-fard, M., and Moghadam, A. J. (2015). Experimental investigation of a PVT system performance using nano ferrofluids. *Energy Conversion and Management*, 103: 468-476.
28. Mohanraj, K., and Sivakumar, G. (2017). Synthesis of γ-Fe_2O_3, Fe_3O_4 and copper doped Fe_3O_4 nanoparticles by sonochemical method. *Sains Malaysiana***,** 46(10): 1935-1942.
29. Mufti, N., Atma, T., Fuad, A., and Sutadji, E. (2014). Synthesis and characterization of black, red and yellow nanoparticles pigments from the iron sand. In *AIP Conference Proceedings,* 1617: 165-169.
30. Song, K., Lee, S., Suh, C.-Y., Kim, W., Ko, K.-S., and Shin, D. (2012). Synthesis and characterization of iron oxide nanoparticles prepared by electrical explosion of Fe wire in Ar–O_2 gas mixtures. *Materials Transactions*, M2012186.
31. Nalle, F., Wahid, R., Wulandari, I., and Sabarudin, A. (2019). Synthesis and characterization of magnetic Fe_3O_4 nanoparticles using oleic acid as stabilizing agent. *Rasayan Journal of Chemistry,* 12(1): 14-21.
32. Xie, L., Qian, W., Yang, S., Sun, J., and Gong, T. (2017). A facile and green synthetic route for preparation of heterostructure Fe_3O_4@Au nanocomposites. *MATEC Web of Conferences*, *88*: 02001.
33. Zhou, J., Meng, L., Lu, Q., Fu, J., and Huang, X. (2009). Superparamagnetic submicro-megranates: Fe_3O_4 nanoparticles coated with highly cross-linked organic/inorganic hybrids. *Chemical Communications*, 42: 6370-6372.
34. Lowry, G. V., Hill, R. J., Harper, S., Rawle, A. F., Hendren, C. O., Klaessig, F., et al. (2016). Guidance to improve the scientific value of zeta-potential measurements in nanoEHS. *Environmental Science: Nano*, *3*(5): 953-965.

35. Bhattacharjee, S. (2016). DLS and zeta potential–what they are and what they are not?. *Journal of Controlled Release,* 235: 337-351.
36. Ostolska, I., and Wiśniewska, M. (2014). Application of the zeta potential measurements to explanation of colloidal Cr_2O_3 stability mechanism in the presence of the ionic polyamino acids. *Colloid and Polymer Science*, *292*(10): 2453-2464.
37. Salopek, B., Krasic, D. and Filipovic, S. (1992). Measurement and application of zeta-potential. *Rudarsko-geolosko-naftni zbornik, 4*(1): 147.
38. Abadeh, A., Passandideh-Fard, M., Maghrebi, M. J. and Mohammadi, M. (2019). Stability and magnetization of Fe_3O_4/water nanofluid preparation characteristics using Taguchi method. *Journal of Thermal Analysis and Calorimetry*, 135(2): 1323-1334.
39. Uskoković, V., Castiglione, Z., Cubas, P., Zhu, L., Li, W. and Habelitz, S. (2010). Zeta-potential and particle size analysis of human amelogenins. *Journal of Dental Research*, 89(2): 149-153.
40. Wang, T., Ni, M., Luo, Z., Shou, C., and Cen, K. (2012). Viscosity and aggregation structure of nanocolloidal dispersions. *Chinese Science Bulletin*, 57(27): 3644-3651.
41. Ghadimi, A., and Metselaar, I. H. (2013). The influence of surfactant and ultrasonic processing on improvement of stability, thermal conductivity and viscosity of titania nanofluid. *Experimental Thermal and Fluid Science*, 51: 1-9.
42. Gensdarmes, F. (2015). Methods of Detection and Characterization. *Nanoengineering,* 2015: 55-84.
43. Wang, L., Wang, X., Gu, R., Wang, H., Yao, L., Wen, L., et al. (2018). Observations of fine particulate nitrated phenols in four sites in northern China: concentrations, source apportionment, and secondary formation. *Atmospheric Chemistry and Physics*, 18(6): 4349-4359.
44. Li, C. H., and Peterson, G. (2006). Experimental investigation of temperature and volume fraction variations on the effective thermal conductivity of nanoparticle suspensions (nanofluids). *Journal of Applied Physics*, 99(8): 084314.
45. Şeşen, M., Tekşen, Y., Şendur, K., Pınar Mengüç, M., Öztürk, H., Yağcı Acar, H., et al. (2012). Heat transfer enhancement with actuation of magnetic nanoparticles suspended in a base fluid. *Journal of Applied Physics*, 112(6): 064320.
46. Abareshi, M., Goharshadi, E. K., Zebarjad, S. M., Fadafan, H. K. and Youssefi, A. (2010). Fabrication, characterization and measurement of thermal conductivity of Fe3O4 nanofluids. *Journal of Magnetism and Magnetic Materials*, 322(24): 3895-3901.
47. Yüksel, N. (2016). The review of some commonly used methods and techniques to measure the thermal conductivity of insulation materials. In A. Almusaed, & A. Almssad (Eds.), *Insulation Materials in Context of Sustainability*. IntechOpen.